ACS Sustainable Chemistry & Engineering

Research Article

Cite This: ACS Sustainable Chem. Eng. 2019, 7, 13668−13679

pubs.acs.org/journal/ascecg

Chemical Transformations in Li-Ion Battery Electrode Materials by Carbothermic Reduction

Gabriele Lombardo,* Burçak Ebin, Mark R. St. J. Foreman, Britt-Marie Steenari, and Martina Petranikova

Department of Chemistry and Chemical Engineering, Industrial Materials Recycling and Nuclear Chemistry, Chalmers University of Technology, SE-412 96, Gothenburg, Sweden

ABSTRACT: The effects of pyrolysis on the composition of the battery cell materials as a function of treatment time and temperature were investigated. Waste of Li-ion batteries was pyrolyzed in a nitrogen atmosphere at 400, 500, 600, and 700 °C for 30, 60, and 90 min. Thermodynamic calculations for the carbothermic reduction of active materials $LiCoO_2$, $LiMn_2O_4$, and $LiNiO_2$ by graphite and gas products were performed and compared to the experimental data. Ni, Mn, and Co (NMC) cathode materials recovered from spent Li-ion batteries were also studied. The results indicate that the organic compounds and the graphite are oxidized by oxygen from the active material and provide the reductive atmosphere. Such removal of the organic components increases the purity of the metal bearing material. Reactions with C and $CO_{(g)}$ led to a reduction of metal oxides with Co, CoO, Ni, NiO, Mn, Mn_3O_4, Li_2O, and Li_2CO_3 as the main products. The reduction reactions transformed the metal compounds in the untreated LiB black mass to more soluble chemical forms. It was concluded that the pyrolysis can be used as an effective tool for the battery waste pretreatment to increase the efficiency of the leaching in hydrometallurgical processing of the black mass. The results obtained can help to optimize the parameters in the industrial processing already used for Li-ion battery recycling, especially if followed by hydrometallurgical treatment. Such optimization will decrease the energy demand and increase the metal recovery rate and utilization of the byproducts.

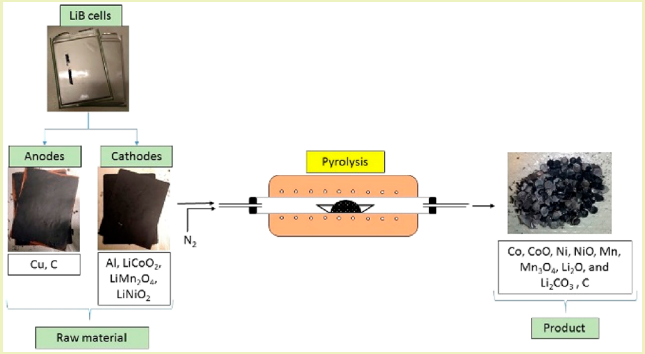

KEYWORDS: *Lithium-ion batteries, Metal recycling, Carbothermic reduction, Pyrolysis, NMC batteries*

INTRODUCTION

Lithium-ion batteries (LiBs) can provide high energy and power per unit of battery weight, which means that they can be made lighter and smaller than other rechargeable batteries.[1] For their performance, LiBs are also widely employed in the car industry for full electric and hybrid engines.[2,3] The International Energy Agency estimates that the demand for lithium batteries is rising: the global electric car stock surpassed the 1 million threshold in 2015 and 2 million in 2016; the forecast indicates that it will range between 9 and 20 million by 2020 and between 40 and 70 million by 2025.[4−6] The increasing use of Li-ion batteries is causing a simultaneous rapid growth in demand for the metals necessary for their production, in particular cobalt (Co), nickel (Ni), manganese (Mn), and lithium (Li). If this trend continues, the current reserves of Co could be depleted in less than 60 years.[7] Co is already a critical raw material due to its economic importance and supply risk.[8] For the Li, no real scarcity is foreseen until 2050 when easily extractable Li reserves in stable countries could decrease significantly. Lithium mining has been associated historically with different forms of institutional risk, such as uncertain mineral rights, conflicting land use, security risks, and other political exposure. This influence is creating instability in the supply and price of Li.[9] Nickel is expected to be less impacted by the increasing use of LiBs than other materials. The annual production is around 2000 kilotons which satisfies primarily the demand for steel production; batteries account for a small fraction of the total.[6] Another critical raw material is graphite,[8] commonly used as an anode active material in LiBs. The natural graphite used for battery production is mainly supplied by a few countries (China, Canada, and Madagascar) and has limited availability.[10] Thus, due to the forecasts about the increasing demand for LiB raw materials, the critical reserves, and the instability in supply and price of these materials, it is important that efficient and cost-effective recycling methods for LiB materials are developed. The work presented in this paper was carried out as a contribution to that development.

BACKGROUND

A lithium-ion battery is made of five principal components: anode, cathode, separator, electrolyte, and current collector. The negative electrode (anode) is composed of a Cu foil coated with graphite; the positive electrode (cathode) is an Al foil covered

Received: December 13, 2018
Revised: May 21, 2019
Published: July 17, 2019

DOI: 10.1021/acssuschemeng.8b06540
ACS Sustainable Chem. Eng. 2019, 7, 13668−13679

with an electrochemically active material.[11] The active material is generally a lithium-transition-metal-oxide $LiMO_2$, (where M stands for Co, Ni, Mn, Al) or NMC materials (Ni, Mn, and Co) and NCA (Ni, Co, and Al), with different ratios between particular metals.[12,13] The adhesion between the Al foil and the active material is improved by a polymeric binder, most often polyvinylidene fluoride (PVDF).[14] The electrodes are kept separate by a separator layer made of polypropylene (PP) or polyethylene (PE).[15] The ion conductivity is facilitated by an electrolyte.[1,16,17] Typical electrolytes include mixtures of alkyl carbonates[18] and Li salts, such as $LiPF_6$.[19]

The recycling processes used at present are mostly focused on the recovery of Co, Ni, and Cu. The increasing demand for LiBs makes it necessary to include also recycling of the Li in order to ensure a long-term sustainability of the LiBs technology.[19,20] There are several recycling technologies available on the market, which include a hydrometallurgical approach (e.g., Recupyl in France) or a combination of smelting and hydrometallurgy applied by Umicore in Belgium, and Nickelhütte in Germany, or intergration of pyrolysis followed by hydrometallurgy used by REDUX and Accurec in Germany. An example of a combined process is ultra high temperature (UHT) applied by Umicore, which involves a plasma technology followed by hydrometallurgical separation of the metals from the alloy of Co−Ni−Fe−Cu.[21−23] Hydrochloric or sulfuric acid are most commonly used for the leaching, due to low costs and high effectivity.[24] Hydrogen peroxide is added to reduce Co, Ni, and Mn compounds to species that have a higher solubility.[25] The recovery of the pure metals is obtained through solvent extraction processes and precipitation.[26,27]

STATE OF THE ART

Current trends in the recycling of Li-ion batteries aim toward the use of thermal pretreatment as an effective tool for battery discharging, electrolyte decomposition, and improvement of the mechanical separation via binder removal. Such pretreatment can be performed using pyrolysis in an inert gas or in vacuum or incineration can be applied. Several papers dealing with such approaches have been published recently. The incineration has been studied in several cases. Results showed a high efficiency in organic component removal with positive effects on Co and Li leaching. A partial decomposition of the cathode material ($LiCoO_2$) into Co_3O_4 at 500 °C and into Co_3O_4 and CoO at 700 °C was observed after 60 min of treatment.[28] A complete removal of the carbon content in $LiCoO_2$ batteries was obtained after a calcination for 5 h. It was reported that Li leaching efficiency increased after carbon removal since carbon acted as an absorbent of lithium ions and thus inhibited the lithium leaching.[29] An improvement in Co and Li recovery rate after incineration at 700 °C was also reported by Petranikova et al.,[28] as well as by Shin et al.[30] due to $LiCoO_2$ reduction and carbon removal. A further increase of the temperature has been reported to instead limit the extraction due to melted aluminum foils covering the $LiCoO_2$ particles.[30] Pyrolysis has been investigated as an alternative treatment method. It is a "greener" process compared to incineration: the concentration of CO and CO_2 per time unit is lower. It was observed that it is possible to efficiently remove the binder (PVDF) and to decompose $LiCoO_2$ into CoO and Li_2O by pyrolyzing the cathodes at 600°C under vacuum for 30 min.[31] When performing a pyrolysis at higher temperature (800 and 1000 °C) and in the presence of graphite, a mixture of Co and Li_2CO_3 was obtained.[32] Xiao and co-workers[33] exposed a mixture of $LiMn_2O_4$ and graphite to a thermal treatment at 800 °C in vacuum conditions. $LiMn_2O_4$ decomposed to Li_2CO_3 and MnO. Work by Georgi-Maschler and co-workers[34] also included utilization of pyrolysis as a tool for discharging the batteries cells. Pyrolysis was performed in a resistance heated retort furnace at temperatures of maximum 250 °C. To improve the separation of active material from the foils, pyrolysis was performed by Zhang and co-workers at 500 °C followed by ultrasonic cleaning and flotation.[35] A significant contribution of that work is the analysis of the pyrolysis products. It was reported that fluorine-containing benzene and ester electrolyte were the main constituents. The $LiCoO_2$ recovery yield improved from 74% to 97% by pyrolysis-ultrasonic-assisted flotation. In comparison to incineration and pyrolysis, where Li stays in the black mass, smelting of LiBs leads to a loss of Li into slag. Chlorination roasting was performed to selectively recover Li from the slag. The evaporation rate of Li was rising with the increase of temperature and the time of chlorination roasting.[36,37] By treating the slag at 1000 °C for 90 min, the evaporation yield of Li reached >97%. Despite high recovery yields, the method is energy demanding. The used reagents can also cause corrosion of the equipment.[38]

Even though thermal pretreatment has been applied or studied in several works, the majority of the research is focused on $LiCoO_2$ as the active material while the current trends are toward NMC and materials with higher Ni content. Moreover, only a limited number of studies focused on thermal treatment of the other type of active materials such as $LiNiO_2$ or $LiMn_2O_4$, which might be used as an alternative to $LiCoO_2$ for the future battery chemistries. There is still a lack of information on the generation of secondary waste during the thermal treatment, characterization of the waste and environmental risk assessment of the gas and oil products remaining after the incineration and pyrolysis. Despite the utilization of pyrolysis/incineration in the industrial LiBs recycling, conditions used are mostly applied as an estimation of the need to reach some process efficiency, without the consideration of energy demand optimization or the adverse effects of the selected treatment on the material recycling efficiency and waste generation.

There is also limited knowledge of the effects of the treatment on the active materials and their recovery via hydrometallurgical methods, which inhibit potential optimization of the processing and thus higher metal recovery rates with lower environmental impact.

Since larger volumes of spent car batteries are expected to reach the recycling market in a few years and combined approaches applying thermal pretreatment and hydrometallurgical processing will be the future trend, optimization of each step is more than crucial for the future sustainable recycling. This work provides a detailed study of the thermal treatment of spent car LiBs with additional information about the effects of the treatment on the other battery chemistries. Modeling and simulation applied provides an insight in the reactions occurring between the active material and the gas phase constituents.

AIM OF THE PRESENT WORK

In this work, pyrolysis of NMC-LiBs, i.e. batteries whose cathode active material has the general composition $Li(Ni_{1/2-y}Mn_{1/2-y}Co_{2y})O_2$, was performed. Based on a thorough literature review, no published investigations where the effects of high temperature on a mixture of both cathode and anode materials of a commercial NMC battery were examined were found. It was expected that, through the carbothermic reduction mechanism, it would be possible to obtain Co, Mn, Ni, and Li in

DOI: 10.1021/acssuschemeng.8b06540
ACS Sustainable Chem. Eng. 2019, 7, 13668−13679

a lower oxidation and/or more soluble state, and thus improve their leaching. Since the thermodynamic databases available do not contain information about the thermodynamic data for the specific NMC active material that we treated, in our theoretical modeling we considered the black mass as a homogeneous mixture of $LiMn_2O_4$, $LiCoO_2$, and $LiNiO_2$, which are three of the most common cathode materials. It is expected that the treatment will cause the removal of the organic binder (polyvinylidene fluoride, PVDF) and so facilitate the separation of the black mass from the current collector by a mechanical treatment. With such an approach, the hydrometallurgical process could be significantly further simplified thus avoiding the presence of Cu and Al in the solution. Since those components would be recovered separately, the number of steps in the hydrometallurgical process could be reduced.

MATERIALS AND METHODS

This work was performed on lithium battery cells provided by Volvo Car Corporation. A total of six cells were dismantled by removing the plastic cover. Cathodes and anodes were manually separated from the separators. The black mass was scraped from the anode copper foils and cathode aluminum foils. Separated components were weighted. This procedure was done to do qualitative and quantitative analysis of the battery cells. For the pyrolysis experiments, crushed mixed battery waste with a separator was used.

Pyrolysis. A quartz tube, with dimensions 700 mm length and 30 mm diameter with a cone 34/35 and socket 34/35, was inserted in a tubular furnace (Nabertherm GmbH Universal Tube Furnace RT 50-250/11) and thermally insulated. A constant flow of nitrogen was used inside the tube, a flowmeter was used to regulate the gas flow at the entrance of the system, and the outgoing gas was bubbled through a glass cylinder filled with 100 mL of Milli-Q water. The furnace heating rate was set to 10 °C/min, and a gas flow of around 340 mL/min was used.

The plastic cover of the six cells was opened, and electrodes were collected. Representative samples were obtained by pressing a puncher with a circular shape of diameter 2 mm through an equal number of cathodes and anodes. The samples were heated at 400, 500, 600, and 700 °C. The choice of this temperature range was the result of a compromise: at a lower temperature, the efficiency of the PVDF removal, and so the purity of the treated black mass, should be lower than it would be in a treatment at a higher temperature. On the other hand, higher temperatures can cause melting of the Al (660.3 °C), which in liquid state would cover the samples inhibiting the PVDF removal and the contact between the battery and the reductive atmosphere in the oven. It was chosen to perform treatment at 700 °C to observe if at this temperature there are effects of the melting of the Al. To reach the desired temperature, the sample was inserted in the tube to the center of the oven and kept there for 15, 30, 45, 60, 90, and 180 min, respectively. After the chosen heating time, the heating and the gas flow were shut down, and the sample was moved near to the end to stay in the reductive atmosphere while cooling down. The loss in sample weight was examined by weighing the samples before and after the experiment. Experiments were carried out in triplicate.

Standard samples composed of a mix of graphite and one of the pure metal oxides present in the black mass ($LiCoO_2$, $LiMn_2O_4$, and $LiNiO_2$), respectively, were subjected to the same thermal treatment. These standards were analyzed and compared with the other samples in order to identify the mechanism of decomposition of each metal oxide and so confute or confirm the thermodynamic considerations.

Determination of Metal Concentrations in Solid Samples by ICP Analysis. An iCAP 6000 Series ICP-OES was used to determine metal concentrations in the electrodes before and after the thermal treatment for the samples treated at 30, 60, and 90 min. Three samples for each condition of treatment and for the untreated material were dissolved using aqua regia (Merck Millipore nitric acid 65%−EMD Millipore hydrochloric acid 37%) as a leaching agent and applying a temperature of approximately 80 °C and using magnetic stirring. After dissolution, the samples were filtered. The solid sample, remaining on the filter, was washed, dried, and weighed to obtain quantitative and, with X-ray diffraction (XRD) analysis, qualitative information about the undissolved fraction. Dilution of the samples was done using a solution 0.5 M HNO_3.

X-ray Powder Diffraction Qualitative Analysis of Crystalline Compounds−XRD. The XRD analyses were carried out using an X-ray diffractometer Siemens D5000, applying an accelerator voltage of 40 kV and a current of 40 mA. The X-ray wavelength used corresponds to the characteristic Cu K radiation, and a 2θ range from 10° to 80° was included in the scans. Furthermore, sample rotation with a rotation speed of 15 rpm was used in order to avoid the effect of preferential orientation of crystals giving incorrect peak heights.

The obtained diffraction data was evaluated by comparison with standard data for known compounds in the JCPDS database.[39] This method allows for the identification of crystalline compounds present in concentrations of ca. 2 wt %. Amorphous compounds cannot be identified.

Thermodynamic Considerations. The software HSC Chemistry 9, developed by Outotec, was used to carry out thermodynamic calculations, in order to propose a hypothesis about which reaction mechanisms were involved during the thermal treatment. Then, the consistency of these theoretical results was investigated comparing them with the experimental results, which were mostly supported by the XRD analysis of the samples after the thermal treatment. The significance of the thermodynamic consideration lays in the possibility to model the system and predict the possible outcome. Since the main goal of the thermal treatment is the reduction of the complex oxides and determination of the effects of the carbon, thermodynamic modeling was used as a tool to further understand and interpret achieved results and further to select and predict optimal conditions of the thermal treatment.

Analysis of Carbon Content Based on Combustion in O_2. A LECO CS744 instrument was used for the determination of the carbon content in the samples before and after pyrolysis.

Preliminary Tests for the Production of Fluorine Containing Dioxins in the Pyrolysis. A concern existed that fluorine containing dioxin analogues could be formed during the pyrolysis of the battery waste. Therefore, the tar that condensed in the pyrolysis apparatus was extracted with acetone. After filtration the acetone was removed in vacuum before the semisolid residue was extracted with hexane. Both the hexane extract and a solution of the hexane insoluble solids were examined with gas chromatography−mass spectroscopy. As the synthesis and gas chromatography of 2,3,7,8-tetrafluorodibenzo[b,e]-[1,4]dioxine (2,3,7,8-TFDD) has been reported by Weber and co-workers, we searched the GCMS data for ions at 256 M^+, $(M-47)^+$, and $(M-56)^+$ which were the ion masses that Weber and co-workers used for identification.[40]

RESULTS AND DISCUSSION

Characterization of the Battery Material. Starting from five LiB cells, the average weight of each cell was 553.1 ± 0.2 g. It consisted of 19 layers of anode material and 18 layers of cathode material. The weight of the plastic cover was 23.0 g ± 0.9. The weight of the black mass recovered from the cathode was approximately 218.2 g and represents the main component, followed by graphite (115.9 g), copper foils (57.0 g), aluminum foils (36.0 g), and separators (42.2 g). A summary of this data can be seen in Table 1.

The percentage of electrolyte is a calculated value. The electrolyte quickly evaporates during the dismantling which makes it difficult to evaluate its quantity.

The concentrations of the metals in the battery, obtained through ICP-OES analysis, are given in Table 2.

The compositions of the two types of electrodes are, as expected, considerably different (Table 3): Cu was detected only in the anode; Al, Co, Mn, and Ni in the cathode, whereas Li is present in both electrodes. The microstructural study of the

DOI: 10.1021/acssuschemeng.8b06540
ACS Sustainable Chem. Eng. 2019, 7, 13668−13679

Table 1. Average Percentage and Mass of Li-Ion Battery Components Per Battery Cell

		weight (g)	weight (%)
anode	copper foil	62.2 ± 0.1	11
	graphite	115.9 ± 0.3	21
cathode	aluminum foil	38.5 ± 0.1	7
	black mass	218.2 ± 0.8	39
polypropylene separator		42.2 ± 0.5	8
electrolyte			15

mixed material from both electrodes performed by XRD identified the presence of Cu and Al in metal form and in the form of their oxides (Figure 1a). The most intense peak at 27° is generated by the graphitic carbon. The complexity and, in some cases, similarity of the spectra for transition metal oxides makes it difficult to get an identification of the specific Co, Ni, and Mn oxides present. Therefore, further XRD analysis was performed on only the cathode active material, which was mechanically separated from the aluminum layer (Figure 1b).

The peak at 18.7° is common for all three lithium containing metal oxides expected. Therefore, the presence or absence of this peak in the diffractogram of the treated samples can be used to confirm a complete decomposition of the lithium metal oxides in the treatment steps.

The XRD spectra of the solid fractions remaining after the attempted total dissolution of the samples shows a hump at low angles. This is due to the amorphous nature of the polymers, i.e. the separator material that most commonly is polypropylene and the PVDF. When dissolving cathodes and anodes separately, it was observed that the undissolved fraction obtained from the negative electrodes is essentially graphite. The spectrum of the cathode shows the signal produced by the separator material, polypropylene (PP). It was not possible to distinguish the signal of the PVDF because of its amorphous state. The signal of Al_2O_3 was also detected. This oxide is formed by the natural oxidation of the surface of the aluminum foil and is particularly resistant to acid attack even by the aqua regia.

Thermodynamic Considerations. The carbon present in the samples triggers a carbothermic reduction of metal oxides through the gaseous intermediate CO. There is no data in the HSC Chemistry database available for NMC compounds so, as an approximation, the oxides were considered individually and their possible interactions with C and CO were studied theoretically at temperatures between 300 and 800 °C and standard pressure.

$LiCoO_2$ is stable at temperatures below 850 °C. At a temperature higher than 300 °C, C and CO can reduce this metal oxide to Co and CoO through reactions 1−3. The plot in Figure 2 shows how ΔG^0 varies with temperature for reactions 1−5.

$$4LiCoO_2(s) + 3C(s) \rightarrow 2Li_2O(s) + 4Co(s) + 3CO_2(g) \quad (1)$$

$$4LiCoO_2(s) + C(s) \rightarrow 2Li_2O(s) + 4CoO(s) + CO_2(g) \quad (2)$$

$$2LiCoO_2(s) + 3C(s) \rightarrow Li_2O(s) + 2Co(s) + 3CO(g) \quad (3)$$

$$2LiCoO_2(s) + C(s) \rightarrow Li_2O + 2CoO(s) + CO(g) \quad (4)$$

$$2LiCoO_2(s) + 3CO(g) \rightarrow Li_2O(s) + 2Co(s) + 3CO_2(g) \quad (5)$$

Increasing the temperature promotes the reactions of $LiCoO_2$ with C. On the other hand, the interaction of $LiCoO_2$ with CO as described by reaction 2 is only slightly influenced by a variation in the temperature and appears to be the most favorable up to 700 °C. Around this temperature, the three reactions become competitive, with $\Delta G^0 \approx -128$ kJ. Through the spontaneous reactions 6 and 7, CoO can react further with C and CO and have Co and CO_2 as products:

$$C(s) + 2CoO(s) \rightarrow 2Co(s) + CO_2(g) \quad (6)$$

$$CO(g) + CoO(s) \rightarrow Co(s) + CO_2(g) \quad (7)$$

To summarize: the results show that Li tends to keep its oxidation state and form the stable Li_2O whereas Co tends to be reduced from oxidation state 3+ to 2+ or even further to Co metal. Graphite is converted in CO and CO_2. The possible reaction between CO_2 and Li_2O has Li_2CO_3 as product as described by eq 8. This reaction has a $\Delta G^0 = 0.14T - 174.58$ (0−1000 °C) so the slope is positive but the reaction is thermodynamically permitted because its ΔG^0 remains negative in the considered temperature range.

$$CO_2(g) + 2Li_2O(s) \rightarrow Li_2CO_3(s) \quad (8)$$

Thus, Co and Li_2CO_3 can be the main solid products of the carbothermic reduction. $LiCoO_2$ can react with C and CO and form Co, Li_2CO_3, and gases (CO and CO_2), through the following reactions:

$$2LiCoO_2(s) + 3CO(g) \rightarrow 2Co(s) + Li_2CO_3(s) + 2CO_2(g) \quad (9)$$

$$6LiCoO_2(s) + 5C(s) \rightarrow 6Co(s) + 3Li_2CO_3(s) + CO_2(g) + CO(g) \quad (10)$$

Based on the above considerations, reaction 10 is the most favorable thermodynamically and it is plotted in Figure 2 as described by equation $\Delta G^0 = -0.58T - 211.97$ (0−1000 °C).

Thermodynamic data related to $LiMn_2O_4$ were not available in the HSC 9 database. Therefore, a separate database was created using the entropy and heat capacity data published by Knyazev[41] and enthalpy data published by Lai.[42] These extensions of the database permitted the extrapolation of ΔG^0 until 126.85 °C. Beyond that temperature, the thermodynamic parameters were correlated using the same software.

The calculation shows that $LiMn_2O_4$ would not spontaneously decompose in the chosen range of temperature. The reactions with C or CO have Mn_3O_4, Li_2CO_3, and Li_2O as products, as described by (11) and (12). Mn with oxidation states +3 and +4 in $LiMn_2O_4$ are reduced to Mn with oxidation states +2 and +3 in Mn_3O_4. The thermodynamic plots of ΔG^0

Table 2. Mass Percent of Metals in the Average Battery Cell

Mn	Ni	Co	Cu	Li	Al
11.0 ± 0.7	5.6 ± 0.3	5.5 ± 0.3	12.3 ± 0.8	2.4 ± 0.2	6.8 ± 0.5

DOI: 10.1021/acssuschemeng.8b06540
ACS Sustainable Chem. Eng. 2019, 7, 13668−13679

Table 3. Mass Percent of Metals in the Respective Electrode Material

element	Mn	Ni	Co	Cu	Li	Al
anode	nd[a]	nd	nd	27.2 ± 0.8	0.1 ± 0.2	0.00
cathode	19.0 ± 0.7	9.0 ± 0.3	9.1 ± 0.3	nd	3.7 ± 0.2	10.3 ± 1.2

[a]Not detected.

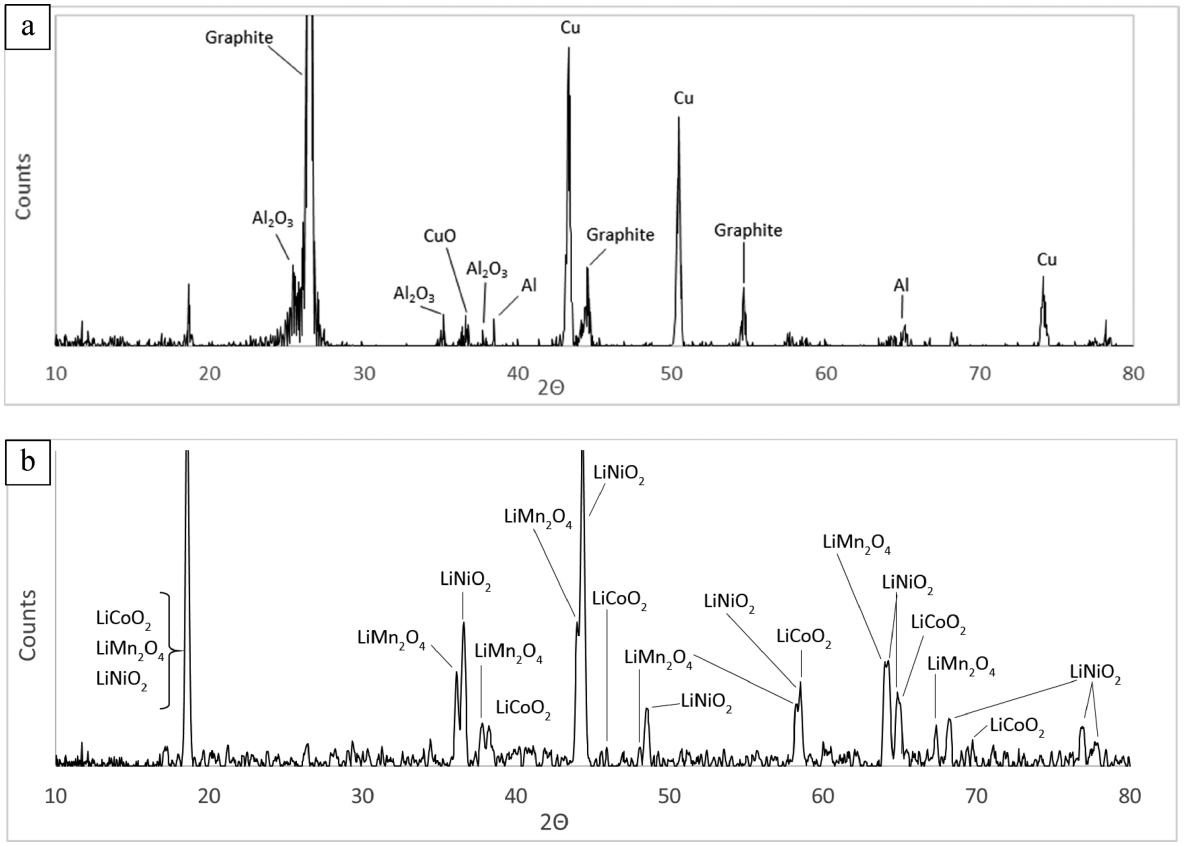

Figure 1. (a) X-ray diffractogram of an untreated sample containing material from both anode and cathode. (b) X-ray diffractogram of a sample of untreated battery cathode black mass.

versus T for these reactions are shown in Figure 3. Mn with oxidation states +3 and +4 can also be reduced by C to give MnO and CO as products, as described by reaction 13. This reaction has a more negative slope for the curve describing the dependence of Gibbs free energy on T, compared to those of reactions 9 and 10. This curve can be described by the equation $\Delta_r G_T^0 = -0.227T - 138.62$. Li is not reduced and forms the Li_2CO_3.

$$2.4LiMn_2O_4(s) + C(s) \rightarrow 1.2Li_2O(s) + 1.6Mn_3O_4(s) + CO_2(g) \quad (11)$$

$$3LiMn_2O_4(s) + 2.5CO(g) \rightarrow 2Mn_3O_4(s) + 1.5Li_2CO_3(s) + CO_2(g) \quad (12)$$

$$2LiMn_2O_4(s) + 2C(s) \rightarrow Li_2CO_3(s) + 4MnO(s) + CO(g) \quad (13)$$

MnO could theoretically be oxidized to Mn_3O_4 through the reaction with $LiMn_2O_4$, as described by (14). However, this oxidation is not thermodynamically permitted since the Gibbs free energy is positive in all the considered temperature range. Instead, MnO can act as a reducing agent in the carbothermic reaction of $LiMn_2O_4$ as shown in (15) and (16). The reaction with CO is significantly affected by the presence of MnO with a decrease of the ΔG^0 compared to that of reaction 12.

$$2LiMn_2O_4(s) + 5MnO(s) \rightarrow Li_2O(s) + 3Mn_3O_4(s) \quad (14)$$

$$2.8LiMn_2O_4(s) + MnO(s) + C(s) \rightarrow 1.4Li_2O(s) + 2.2Mn_3O_4(s) + CO_2(g) \quad (15)$$

$$4LiMn_2O_4(s) + MnO(s) + 3CO(g) \rightarrow 2Li_2CO_3(s) + 3Mn_3O_4(s) + CO_2(g) \quad (16)$$

This means that MnO can be involved in the reduction of the $LiMn_2O_4$ but C and CO would be the main reducing agents.

There is not enough data in the HSC Chemistry database available for $LiNiO_2$, but its behavior was modeled as being similar to that of $LiCoO_2$. The carbothermic reduction can have Ni, NiO, and Li_2CO_3 as main products. The NiO can in its turn be reduced by C and CO into Ni with an associated formation of CO_2, as described by reactions 18 and 19. The corresponding plot of ΔG^0 as a function of T is shown in Figure 4.

DOI: 10.1021/acssuschemeng.8b06540
ACS Sustainable Chem. Eng. 2019, 7, 13668−13679

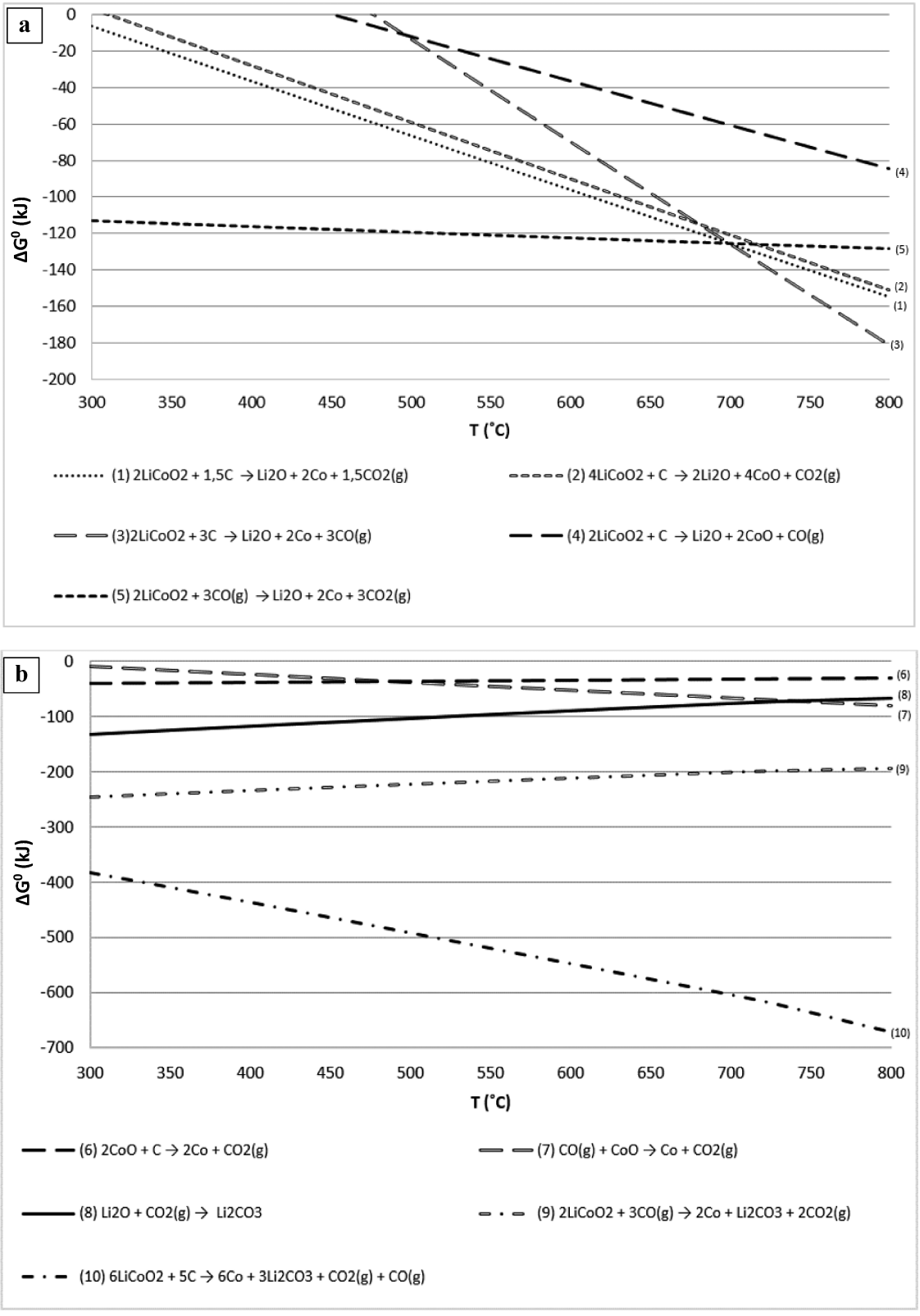

Figure 2. Plot of the ΔG^0 (kJ) vs T (°C) for reduction of $LiCoO_2$ with C or CO.

$$4LiNiO_2(s) + C(s) \rightarrow 2Li_2O(s) + 4NiO(s) + CO_2(g) \quad (17)$$

$$2LiNiO_2(s) + 3C(s) \rightarrow Li_2O(s) + 2Ni(s) + 3CO(g) \quad (18)$$

$$2LiNiO_2(s) + C(s) \rightarrow Li_2O(s) + 2NiO(s) + CO(g) \quad (19)$$

$$2LiNiO_2(s) + 3CO(g) \rightarrow 2Ni(s) + Li_2CO_3(s) + 2CO_2(g) \quad (20)$$

DOI: 10.1021/acssuschemeng.8b06540
ACS Sustainable Chem. Eng. 2019, 7, 13668−13679

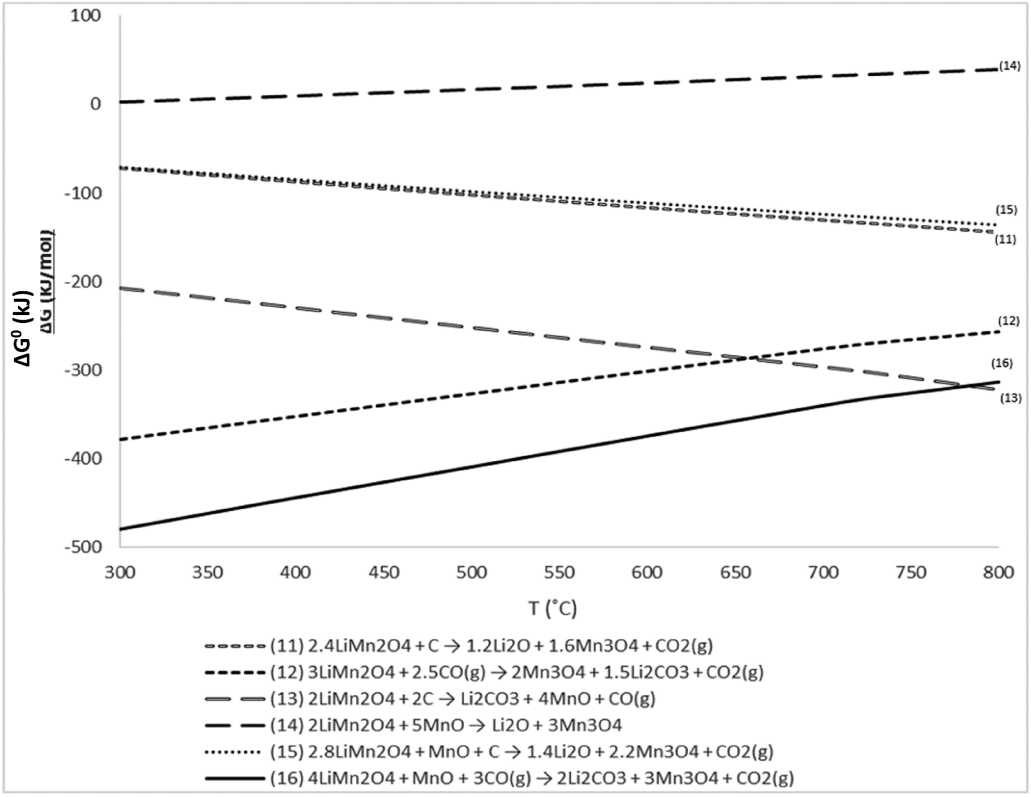

Figure 3. Plot of the ΔG^0 (kJ) vs T (°C) for the most thermodynamically favored reactions of decomposition of $LiMn_2O_4$.

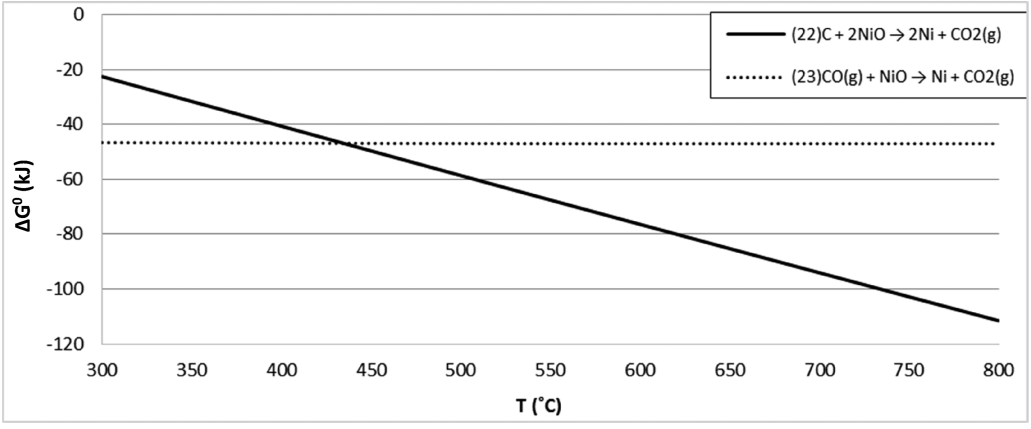

Figure 4. Plot of the ΔG^0 (kJ) vs T (°C) for the carbothermic reduction of NiO.

$$6LiNiO_2(s) + 5C(s) \rightarrow 6Ni(s) + 3Li_2CO_3(s) + CO_2(g) + CO(g) \quad (21)$$

$$C(s) + 2NiO(s) \rightarrow 2Ni(s) + CO_2(g) \quad (22)$$

$$CO(g) + NiO(s) \rightarrow Ni(s) + CO_2(g) \quad (23)$$

Pyrolysis Results. The variation of the weight of the samples (Δw %) during the pyrolysis experiments (Figure 5) shows that the weight loss increases with the rise of the temperature and the duration of the thermal treatment. At 700 °C there is a loss of ∼22% during 90 min of treatment which is double the weight loss obtained at 400 °C. Instead, the temperature increase from 500 to 600 °C does not have a notable effect on the sample weight. The Δw % determined by the variation of the treatment time is more evident at 700 °C than at a lower temperature. It varies from ∼9% at 15 min to ∼22% after 180 min. Overall, the Δw % obtained treating the battery cells for 180 min at 400 °C is equal to that obtained at 700 °C for just 30 min. For all samples, a significant part of the weight is lost in the first 15 min of treatment. This can be determined by the evaporation of the organic solvents present in the battery. At each temperature, the Δw % reached a maximum after 90 min, follow by a plateau. The results of the samples treated at 500 and 600 °C did not show a significant difference after 180 min considering the standard deviation resulting from the heterogeneous character of the material.

The weight loss is mainly caused by the production of volatile organic species during the decomposition of the organic components of the battery cells. The ICP-OES data in Table 4 show a general increase in the concentration of the metals in the sample with the increasing temperature and time of treatment.

DOI: 10.1021/acssuschemeng.8b06540
ACS Sustainable Chem. Eng. 2019, 7, 13668−13679

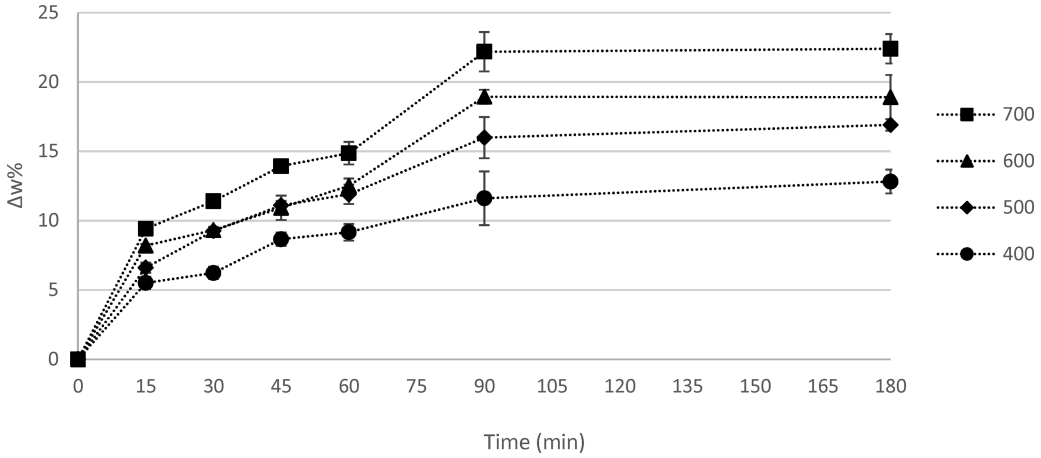

Figure 5. Plots that show the weight loss in experiments at different temperatures and times. The point (0; 0) correspond to the untreated material.

Table 4. Percent Weight of Each Element in the Untreated and Thermal Treated Samples

		% w					
T (°C)	time (min)	Mn	Ni	Co	Cu	Li	Al
untreated		11.0 ± 0.7	5.6 ± 0.3	5.5 ± 0.3	12.3 ± 0.8	2.4 ± 0.2	6.8 ± 0.5
400	30	11.4 ± 0.3	6.0 ± 0.3	5.7 ± 0.3	12.9 ± 0.1	2.6 ± 0.3	7.1 ± 0.3
	60	11.6 ± 0.2	6.2 ± 0.3	5.8 ± 0.1	13.1 ± 0.2	2.6 ± 0.1	7.3 ± 0.1
	90	11.8 ± 0.2	6.3 ± 0.3	5.9 ± 0.3	13.4 ± 0.3	2.7 ± 0.3	7.4 ± 0.3
500	30	11.7 ± 0.3	5.9 ± 0.3	5.7 ± 0.3	13.0 ± 0.3	2.8 ± 0.2	6.0 ± 0.3
	60	12.8 ± 0.5	6.1 ± 0.3	6.3 ± 0.3	13.4 ± 0.2	2.8 ± 0.3	7.1 ± 0.2
	90	13.2 ± 0.3	6.7 ± 0.3	6.6 ± 0.3	15.3 ± 0.1	3.1 ± 0.3	7.5 ± 0.3
600	30	11.7 ± 0.2	6.2 ± 0.3	5.7 ± 0.3	12.5 ± 0.1	2.7 ± 0.2	7.4 ± 0.3
	60	12.6 ± 0.1	6.3 ± 0.1	6.1 ± 0.1	13.6 ± 0.2	2.4 ± 0.3	7.3 ± 0.3
	90	13.2 ± 0.3	6.7 ± 0.3	6.6 ± 0.3	14.4 ± 0.3	3.1 ± 0.3	9.9 ± 0.3
700	30	12.0 ± 0.1	6.5 ± 0.1	5.9 ± 0.1	13.6 ± 0.3	2.9 ± 0.1	8.2 ± 0.1
	60	12.2 ± 0.1	7.0 ± 0.3	6.2 ± 0.3	14.3 ± 0.1	3.0 ± 0.3	10.1 ± 0.1
	90	14.2 ± 0.3	7.1 ± 0.2	6.7 ± 0.3	15.1 ± 0.3	3.0 ± 0.3	10.3 ± 0.2

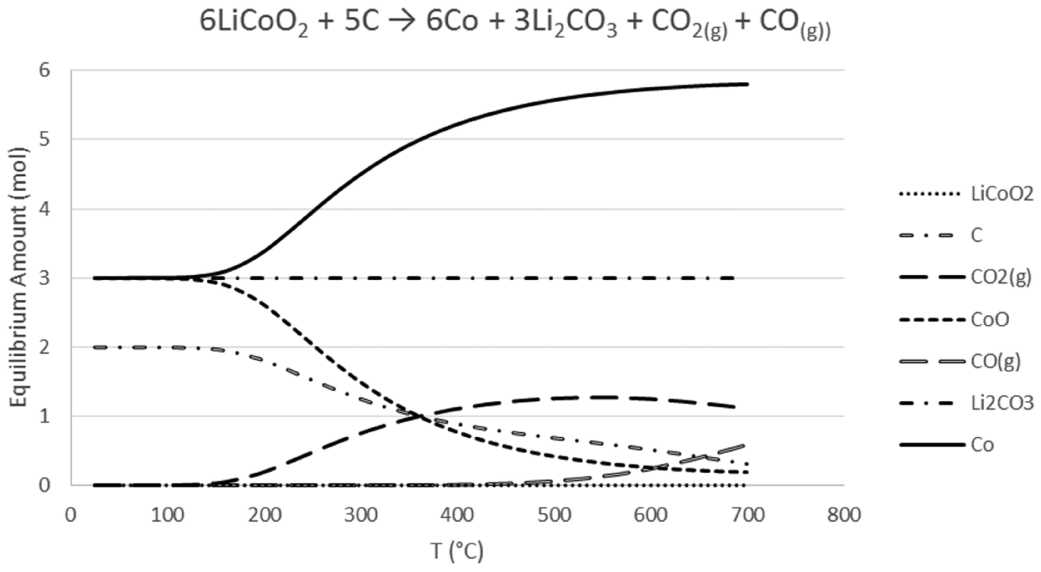

Figure 6. Variation of the equilibrium amount vs temperature for each species involved in the carbothermic reaction of $LiCoO_2$ with C that has Co, Li_2CO_3, and gases (CO and CO_2) as products, as described by (10).

Al, Cu, from the metal foils, and Mn are the most abundant (>10 w %), followed by Co and Ni (~7 w %). Li has an abundance of around 3 w %. As expected, the rise of the metals concentration is almost proportional to the decrease of the weight of the sample. In the samples treated at 700°C for 1.5 h a weight loss equal to ~22% corresponded an increase of metals w % of around ~25%. Al is an exception since its concentration rises almost with 50%.

DOI: 10.1021/acssuschemeng.8b06540
ACS Sustainable Chem. Eng. 2019, 7, 13668−13679

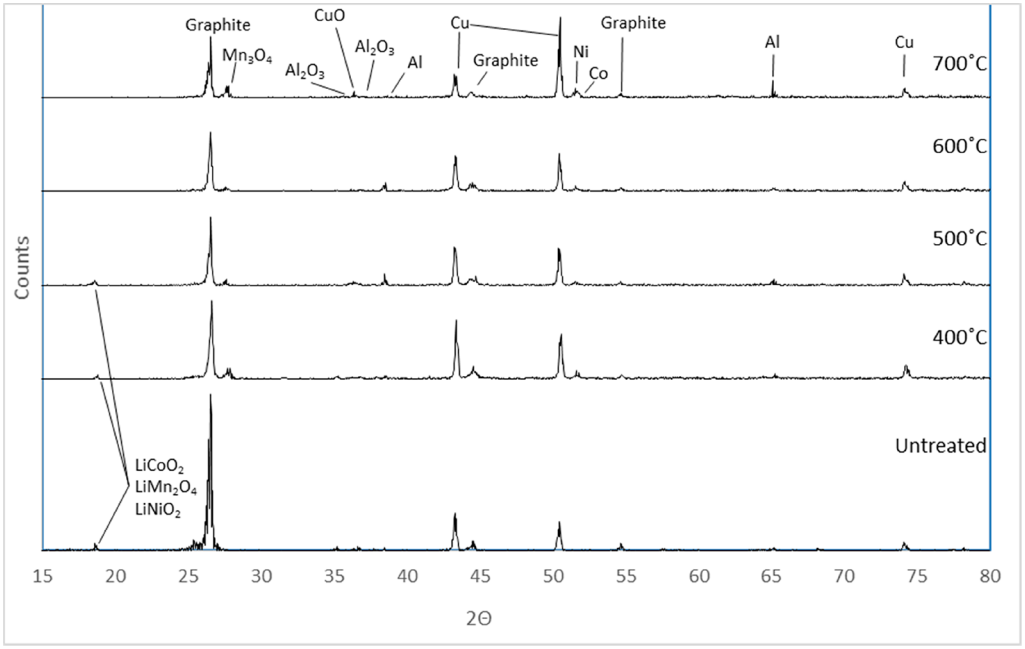

Figure 7. Comparison between the spectra of an untreated sample and the spectra of 1.5 h pyrolyzed samples at 400, 500, 600 and 700 °C.

It was expected that at 700 °C the aluminum layer could melt covering the black mass and limiting the contact with C and CO. However, no effects indicating a possible melting of the Al were observed in the experiments.

The data in both Table 4 and Figure 5 show that the weight of the samples treated at 500 and 600 °C do not differ significantly. This can be explained by the fact that the decomposition of the organic material present in the battery occurs already at 400 °C. In a TGA study of PVDF by Kuila and co-workers, the data exhibited a single degradation at 450 °C, with the material losing more than the 80% of its weight before 500 °C was reached.[43] At higher temperature, oxidation of the C in CO and CO_2 leads to additional weight loss between 600 and 700 °C.

The gas released by the samples during the thermal treatment and the absorption liquid was collected and analyzed, and the results will be presented in a separate paper.

We were not able to find a mass spectroscopy scan for any of the sample fractions which had a spectrum containing the three lines for ion masses 256 M^+, $(M-47)^+$, and $(M-56)^+$ which would identify the fluoro-dioxin 2,3,7,8-TFDD. Even though no evidence for the formation of fluorinated dioxins was found in the present study, their possible existence is an important issue and we will study it further in our continued work.

Figure 6 shows the variation of the equilibrium amount versus temperature for each species involved in the carbothermic reaction of $LiCoO_2$ with C that has Co, Li_2CO_3, and gases (CO and CO_2) as products, as described by (11). These curves are the result of thermodynamic calculations. The data shows that, beyond 500 °C, C forms both CO and CO_2 and the amount of CO grows with increasing of the temperature. This means that at 700 °C, the quantity of C consumed to form CO and CO_2 is significantly higher than at lower temperature. Furthermore, the reactions that have these gases as products are promoted by the constant flow of nitrogen that, removing CO and CO_2 from the system, does not allow the achievement of the reaction equilibrium.

In Figure 7 the XRD spectrum of the untreated battery is compared with the spectra of the samples treated for 1.5 h.

Making quantitative considerations based on these spectra is not correct, but it is evident that an increase of the treatment temperature leads to a decrease of the intensity of the peaks at 26.5°, 43.3°, and 54.9°, which represent the signals emitted by the graphitic carbon. A carbon analyzer was used to quantify the residual carbon in the samples. The sources of carbon are the graphite that covers the anode layer, the separator polymer, the PVDF, and the organic components of the electrolyte.

The concentration of carbon in the original and heat treated battery materials is shown in Table 5. The concentration of carbon in the samples treated at 700 °C for 90 min is the lowest (16 w %), starting from an initial content of 41 wt %. It is probable that this weight loss is caused by a consumption of the graphite and the organic substances during the heating with the formation of CO and CO_2.

Table 5. Variation of the Carbon Concentration in the Sample with the Temperature for the Three Heat Treatment Periods: 30, 60, and 90 min

T (°C)	time	carbon content (%)
untreated		40.8 ± 2.8
400	30 min	35.5 ± 2.4
	60 min	32.8 ± 2.0
	90 min	21.2 ± 1.6
500	30 min	32.0 ± 2.5
	60 min	31.7 ± 2.5
	90 min	23.3 ± 1.2
600	30 min	31.4 ± 1.7
	60 min	29.4 ± 2.5
	90 min	21.1 ± 1.6
700	30 min	27.2 ± 2.5
	60 min	25.2 ± 0.6
	90 min	16.0 ± 1.6

The XRD peaks at 50.5° and 74° describe the presence of metals in elemental form, as Ni, Mn, Cu, and Co formed by the reducing action of the carbon on the metal oxides and salts.

DOI: 10.1021/acssuschemeng.8b06540
ACS Sustainable Chem. Eng. 2019, 7, 13668−13679

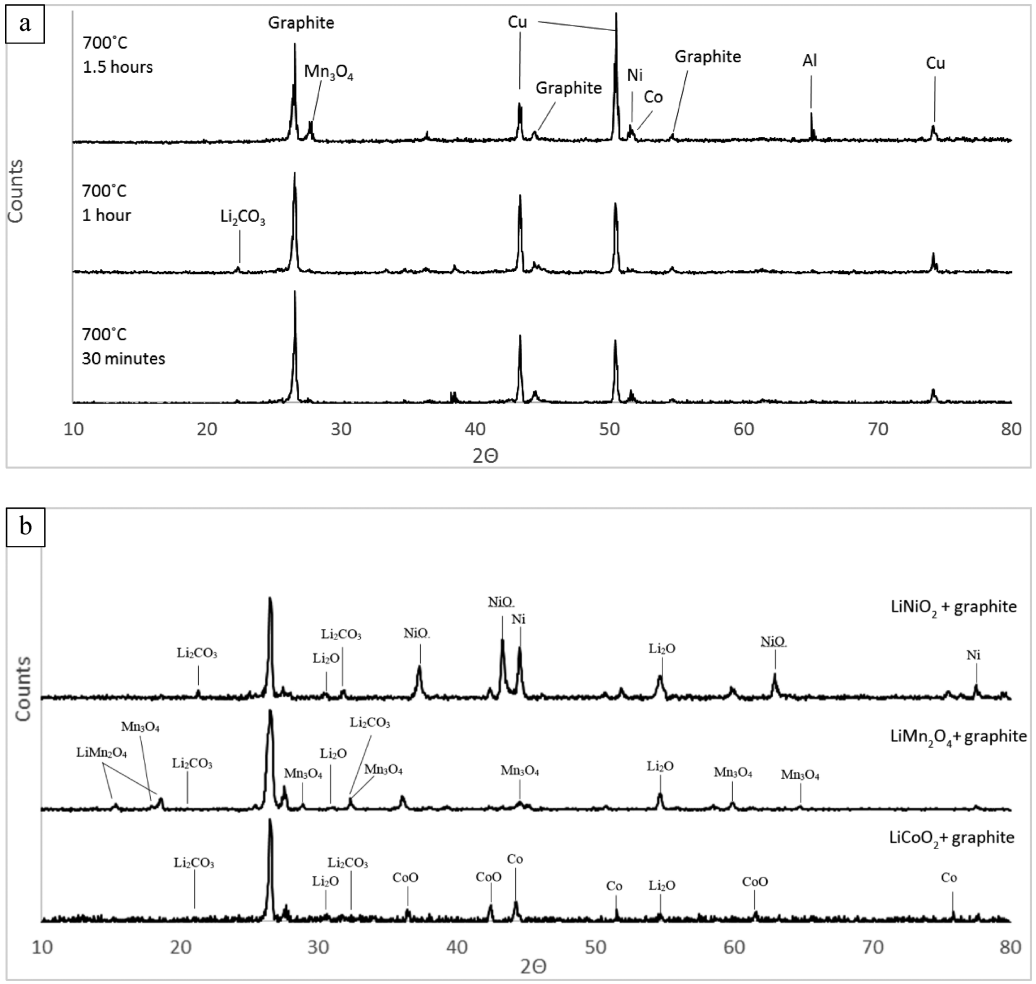

Figure 8. (a) Comparison between spectra of pyrolyzed samples at 700 °C per 30 min, 1 h, and 1.5 h. (b) Comparison of the spectra of standard samples, composed of a mix of graphite and one of the salts present in the black mass, which are $LiCoO_2$, $LiMn_2O_4$, and $LiNiO_2$. All samples were pyrolyzed at 700 °C for 1.5 h.

The diffraction peak at 18.7°, that is common for all three lithium−metal oxides, is present in the diffractogram of the sample that was treated at 500 °C, but it was not detected for the samples treated at higher temperatures (Figure 7). As shown in Figure 8a, it is possible to observe the effect of the increasing time of treatment: at 700 °C, only after 1.5 h, the peak at 18.7° disappear. The treatment at 600 and 700 °C for 1.5 h seem to be sufficient to get an almost complete carbothermic reduction of the active material.

The metal species have diffraction peaks at similar 2θ angles and this limits the data resolution. To get a better identification of the compounds, XRD spectra of standard samples, i.e. pure metal oxides, that had been mixed with graphite and treated in pyrolysis at 700 °C were collected (Figure 8b).

The hypothesis about how the thermal treatment affects different active materials, which are presented in the thermodynamic considerations of this paper, are supported and confirmed by the XRD results. The XRD spectrum of the mixture of $LiCoO_2$ pyrolyzed with an excess of graphite at 700 °C for 1.5 h shows the presence of Li_2O, Li_2CO_3, CoO, and Co. This data confirms that the reactions 9 and 10 correctly describe the carbon induced reduction. The presence of Li_2O and CoO was not expected: even if the reduction of CoO to metal Co with C and CO, described by reactions 6 and 7, is thermodynamically permitted, there has not been a complete transformation in the experiments. The same was observed for the reactions of Li_2O that had not completely reacted with CO_2 to form Li_2CO_3 as described by reaction 8. The reasons can be that the reaction time was shorter than needed (kinetic hindering) and/or that the gas flow that transports CO and CO_2 out of the system is too high which limits the contact between the gas and the solid. Another possible reason is that the samples are heterogeneous mixture of anodes and cathodes, so carbon is not equally distributed in each part of the samples.

The XRD results obtained for reaction products from pyrolysis of a mix of $LiMn_2O_4$ and graphite showed the presence of Li_2O, Li_2CO_3, and Mn_3O_4. Also in this case the thermodynamic considerations were confirmed and reactions 11−16 can be used to describe the reaction mechanism.

The XRD spectra of $LiNiO_2$ confirms that the reaction with CO and CO_2 determines the reduction to NiO and Ni, as described by (22) and (23), and the formation of Li_2O and Li_2CO_3. The time and temperature of treatment did allow a complete decomposition of NiO in Ni and the reaction between the total amounts of Li_2O with CO_2.

CONCLUSIONS

More detailed conclusions from the present work are

DOI: 10.1021/acssuschemeng.8b06540
ACS Sustainable Chem. Eng. 2019, 7, 13668−13679

1. Treating the mix of cathodes and anodes of an NMC-LiB at a temperature between 400 and 700 °C, the C triggers a carbothermic reduction of the cathode active material, obtaining Co, Mn, and Ni, in a lower oxidation and/or more soluble state. Co, CoO, Ni, NiO, Mn, Mn_3O_4, Li_2O, and Li_2CO_3 are the main products, confirming the thermodynamic calculation results.
2. The pyrolysis causes the decomposition of the graphite and organic components, which are hydrophobic and could create difficulties in leaching and solid−liquid separation processes.
3. The increasing of the temperature and time of treatment promotes the carbothermic reduction and the removal of graphite and organic components. It was observed that at 700 °C after 1.5 h of treatment the cathode active material is completely decomposed, and the content of the carbon reaches 16 w %, starting from an initial 41 wt %.

The method that we performed can be applied flexibly on batteries of different chemistry. Pyrolysis is already used as thermal pretreatment in some industrial recycling processes. Results achieved contribute to a better understanding of the effect of carbothermal treatments on the complex chemical system in real battery waste processing and can be applied to optimize the industrial processing to reach higher efficiencies in complex oxides transformation and to decrease the treatment time and so the energy demands for the processing. Our further work will include the development of such a flexible hydrometallurgical process for an economically convenient metal recovery from spent LiB with a different chemistry.

AUTHOR INFORMATION

Corresponding Author

*Email: gablom@chalmers.se.

ORCID

Gabriele Lombardo: 0000-0001-6477-8661

Notes

The authors declare no competing financial interest.

ACKNOWLEDGMENTS

This research was supported by Swedish Energy Agency−Battery fund (Grant No: 40506-1). The authors would like to acknowledge the support of Volvo Cars Corporation for providing the samples and valuable discussion. We also thank the Department of Modeling and Simulation at Outotec for the help with the extending the database data for the thermodynamic calculations.

REFERENCES

(1) Swiatowska, J.; Chagnes, A. *Lithium Process Chemistry Resources, Extraction, Batteries, and Recycling* **2015**, 289.

(2) International Energy Agency. *Oil information: Overview*; 2018; ISBN PDF: 978-92-64-30118-4.

(3) International Energy Agency. *Coal information: Overview*; 2018; ISBN PDF: 978-92-64-30122-1.

(4) Scrosati, B.; Garche, J. Lithium batteries: Status, prospects and future. *J. Power Sources* **2010**, *195*, 2419−2430.

(5) Talens Peiro, L.; Villalba Mendez, G.; Ayres, R. U. Lithium: Sources, Production, Uses, and Recovery Outlook. *JOM* **2013**, *65*, 986−996.

(6) International Energy Agency. *Global EV outlook*; 2017.

(7) Warner, J. *The Handbook of Lithium-Ion Battery Pack Design: Chemistry, Components, Types and Terminology* **2015**.

(8) *Report on Critical Raw Materials for the EU, Report of the Ad hoc Working Group on defining critical raw*; 2017.

(9) Miedema, J. H.; Moll, H. C. Lithium availability in the EU27 for battery-driven vehicles: the impact of recycling and substitution on the confrontation between supply and demand until 2050. *Resour. Policy* **2013**, *38*, 204−211.

(10) Moradi, B.; Botte, G. G. Recycling of graphite anodes for the next generation of lithium ion batteries. *J. Appl. Electrochem.* **2016**, *46*, 123−148.

(11) Watanabe, C. Why Battery Cost Could Put the Brakes on Electric Car Sales. BNEF.com 11/29/2017.

(12) Mizushima, K.; Jones, P. C.; Wiseman, P. J.; Goodenough, J. B. Li_xCoO_2 ($0 < x \leq 1$): a New Cathode Material for Batteries of High Energy Density. *Mater. Res. Bull.* **1980**, *15*, 783−789.

(13) Xu, B.; Qian, D.; Wang, Z. Y.; Meng, Y. S. Recent progress in cathode materials research for advanced lithium ion batteries. *Mater. Sci. Eng., R* **2012**, *73*, 51−65.

(14) Li, L.; Dunn, J. B.; Zhang, X. X.; Gaines, L.; Chen, R. J.; Wu, F.; Amine, K. Recovery of metals from spent lithium-ion batteries with organic acids as leaching reagents and environmental assessment. *J. Power Sources* **2013**, *233*, 180−189.

(15) Hanisch, C.; Diekmann, J.; Stieger, A.; Haselrieder, W.; Kwade, A. Recycling of Lithium-Ion Batteries. *Handbook of Clean Energy Systems* **2015**, 1.

(16) Wakihara, M.; Yamamoto, O. *Lithium ion batteries: fundamentals and performance* **1998**, 127−155.

(17) Romare, M.; Dahllöf, L. *The Life Cycle Energy Consumption and Greenhouse Gas Emissions from Lithium-Ion Batteries*; IVL Swedish Environmental Research Institute, 2017; ISBN: 978-91-88319-60-9.

(18) Zhang, T.; He, Y.; Wang, F.; Ge, L.; Zhu, X.; Li, H. Chemical and process mineralogical characterizations of spent lithium-ion batteries: an approach by multi-analytical techniques. *Waste Manage.* **2014**, *34*, 1051−1058.

(19) Diekmann, J.; Hanisch, C.; Froböse, L.; Schälicke, G.; Loellhoeffel, T.; Fölster, A.; Kwade, A. Ecological Recycling of Lithium-Ion Batteries from Electric Vehicles with Focus on Mechanical Processes. *J. Electrochem. Soc.* **2017**, *164*, A6184−A6191.

(20) Gaines, L. The future of automotive lithium-ion battery recycling: Charting a sustainable course. *Sustainable Materials and Technologies* **2014**, *1-2*, 2−7.

(21) Gaines, L.; Sullivan, J. L.; Burnham, A. Life-Cycle Analysis for Lithium-Ion Battery Production and Recycling. *90th Annual Meeting of the Transportation Research Board*, Washington, DC, 2011.

(22) Cheret, D. Battery collection and recycling. In *Industrial Applications of Batteries. From Cars to Aerospace and Energy Storage*, Broussely, M., Pistoia, G., Eds.; Elsevier B.V: Amsterdam, 2007.

(23) Li, Z.; Huang, J.; Liaw, B. Y.; Metzler, V.; Zhang, J. A review of lithium deposition in lithium-ion and lithium metal secondary batteries. *J. Power Sources* **2014**, *254*, 168−182.

(24) Joulié, M.; Laucournet, R.; Billy, E. Hydrometallurgical process for the recovery of high value metals from spent lithium nickel cobalt aluminum oxide based lithium-ion batteries. *J. Power Sources* **2014**, *247*, 551−555.

(25) Lain, M. J. Recycling of lithium ion cells and batteries. *J. Power Sources* **2001**, *97-98*, 736−738.

(26) Granata, G.; Moscardini, E.; Pagnanelli, F.; Trabucco, F.; Toro, L. Product recovery from Li-ion battery wastes coming from an industrial pre-treatment plant: lab scale tests and process simulations. *J. Power Sources* **2012**, *206*, 393−401.

(27) Lee, C. K.; Rhee, K. I. Preparation of $LiCoO_2$ from spent lithium-ion batteries. *J. Power Sources* **2002**, *109*, 17−21.

(28) Petraníková, M.; Miškufová, A.; Havlík, T.; Forsén, O.; Pehkonen, A. Cobalt recovery from spent portable lithium accumulators after thermal treatment. *Acta Metallurgica Slovaca* **2011**, *2*, 106−115.

(29) Paulino, J.; Busnardo, N.; Afonso, J. Recovery of valuable elements from spent Li-batteries. *J. Hazard. Mater.* **2008**, *150*, 843−849.

DOI: 10.1021/acssuschemeng.8b06540
ACS Sustainable Chem. Eng. 2019, 7, 13668−13679

(30) Shin, S. M. S.; Kim, N. H.; Sohn, J. S.; Yang, D. H.; Kim, Y. H. Development of metals recovery process from Li-ion battery waste. *Hydrometallurgy* **2005**, *79*, 172−181.
(31) Sun, L.; Qiu, K. Vacuum pyrolysis and hydrometallurgical process for the recovery of valuable metals from spent lithium-ion batteries. *J. Hazard. Mater.* **2011**, *194*, 378−384.
(32) Li, J.; Wang, G.; Xu, Z. Environmentally-friendly oxygen-free roasting/wet magnetic separation technology for in situ recycling cobalt.; lithium carbonate and graphite from spent LiCoO2/graphite lithium batteries. *J. Hazard. Mater.* **2016**, *302*, 97−104.
(33) Xiao, J.; Li, J.; Xu, Z. Recycling metals from lithium ion battery by mechanical separation and vacuum metallurgy. *J. Hazard. Mater.* **2017**, *338*, 124−131.
(34) Georgi-Maschler, T.; Friedrich, B.; Weyhe, R.; Heegn, H.; Rutz, M. Development of a recycling process for Li-ion batteries. *J. Power Sources* **2012**, *207*, 173−182.
(35) Zhang, G.; He, Y.; Feng, Y.; Wang, H.; Zhu, X. Pyrolysis-Ultrasonic-Assisted Flotation Technology for Recovering Graphite and LiCoO2 from Spent Lithium-Ion Batteries. *ACS Sustainable Chem. Eng.* **2018**, *6* (8), 10896−10904.
(36) Dang, H.; Wang, B.; Chang, Z.; Wu, X.; Feng, J.; Zhou, H.; Li, W.; Sun, C. Recycled Lithium from Simulated Pyrometallurgical Slag by Chlorination Roasting. *ACS Sustainable Chem. Eng.* **2018**, *6*, 13160−13167.
(37) Barbosa, L. I.; González, J. A.; del Carmen Ruiz, M. Extraction of lithium from *β*-spodumene using chlorination roasting with calcium chloride. *Thermochim. Acta* **2015**, *605*, 63−67.
(38) Lv, W.; Wang, Z.; Cao, H.; Sun, Y.; Zhang, Y.; Sun, Z. A Critical Review and Analysis on the Recycling of Spent Lithium-Ion Batterie. *ACS Sustainable Chem. Eng.* **2018**, *6*, 1504−1521.
(39) *JCP 13: JCPDS−International Center for Diffraction Data*; PDF −4+; Newton Square, PA, 2013.
(40) Weber, R.; Schrenk, D.; Schmitz, H.-J.; Hagenmaier, A.; Hagenmaier, H. Polyfluorinated dibenzodioxins and dibenzofurans — synthesis, analysis, formation and toxicology. *Chemosphere* **1995**, *30*, 629−39.
(41) Knyazev, A. V.; Mączka, M.; Smirnova, N. N.; Knyazeva, S. S.; Chernorukov, N. G.; Ptak, M.; Shushunov, A. N. Study of the phase transition and thermodynamic functions of $LiMn_2O_4$. *Thermochim. Acta* **2014**, *593*, 58−64.
(42) Lai, C.; Chen, J.; Knight, J. C.; Manthiram, A.; Navrotsky, A. Thermodynamic Stability of Transition-Metal-Substituted $LiMn_{2-x}M_xO_4$ (M = Cr.; Fe.; Co.; and Ni) Spinels. *ChemPhysChem* **2016**, *17*, 1973−1978.
(43) Kuila, A.; Maity, N.; Chatterjee, D. P.; Nandi, K. Temperature triggered antifouling properties of poly(vinylidene fluoride) graft copolymers with tunable hydrophilicity. *J. Mater. Chem. A* **2015**, *3*, 13546−13555.

DOI: 10.1021/acssuschemeng.8b06540
ACS Sustainable Chem. Eng. 2019, 7, 13668−13679